Nonequilibrium molecular dynamics calculation of the thermal conductivity based on an improved relaxation scheme

Bing-Yang Cao[a)]
Key Laboratory for Thermal Science and Power Engineering of Ministry of Education, School of Aerospace, Tsinghua University, Beijing 100084, People's Republic of China

(Received 17 March 2008; accepted 21 July 2008; published online 21 August 2008)

A nonequilibrium molecular dynamics (NEMD) method using stochastic energy injection and removal as uniform heat sources and sinks is developed to calculate the thermal conductivity. The stochastic energy is generated by a Maxwell function generator and is imposed on only a few individual molecules each time step. The relaxation of the thermal perturbation is improved compared to other NEMD algorithms because there are no localized heat source and sink slab regions in the system. The heat sources are uniformly distributed in the right half of the system while the sinks are in the left half, which leads to a periodically quadratic temperature distribution that is almost sinusoidal. The thermal conductivity is then easily calculated from the mean temperatures of the right and left half systems rather than by fitting the temperature profiles. This improved relaxation NEMD scheme is used to calculate the thermal conductivities of liquid and solid argons. It shows that the present algorithm gives accurate results with fast convergence and small size effects. Other stochastic energy perturbation, e.g., thermal noise, can be used to replace the Maxwell-type perturbation used in this paper to make the improved relaxation scheme more effective. © *2008 American Institute of Physics*. [DOI: 10.1063/1.2969762]

I. INTRODUCTION

Material thermal conductivities are very important for the designs of industrial processes and are especially important for new nanotechnologies related to energy transport. As "the thermal conductivity has proven to be one of the most difficult transport coefficients to calculate,"[1] many efforts have been put into molecular dynamics (MD) methods over the years to simulate the thermal conductivity of condensed matter. The MD methods for calculating the thermal conductivity can be classified as equilibrium MD (EMD) and nonequilibrium molecular dynamics (NEMD) methods. The EMD methods often use the Green–Kubo method to calculate the time correlation function[2–4] and the equivalent Einstein method to accumulate the displacements in the property.[5] One drawback of the EMD methods is the slow convergence of the long time part of the time correlation function, such that very long time is needed to run simulations for reliable results. One solution is the use of the NEMD methods which impose external perturbation fields (a homogeneous scheme),[6,7] temperature differences,[8,9] heat currents (a reversed scheme),[10,11] transient heat impulsion,[12] or internal thermal noise.[13,14] The NEMD schemes for calculating thermal conductivity have been demonstrated to converge faster than the EMD methods.

A good NEMD algorithm, as discussed in Ref. 10, should exhibit homogeneity and fast convergence, has periodic boundary conditions and small temperature gradient, and satisfies the conservation of energy and momentum and the Hamiltonian. In addition, the relaxation of a thermal perturbation from an imposed heat source (or sink) is also a significant factor like the structural relaxation effects on fluid transport properties.[15] Most NEMD methods for calculating the thermal conductivity construct high and low temperature regions to obtain the thermal current from the hot to the cold. However, the relaxation of the thermal perturbation in the hot and cold slabs may lead to size effects. For molecular fluids, the system size influence is often not important.[16] For solids, however, the size effect becomes significant as a result of phonon scattering in the hot and cold slab regions.[17–19] The hot and cold slabs can be regarded as virtual walls in the simulation system due to the slow relaxation of the thermal perturbation, which worsens the simulation homogeneity and the periodicity of the boundary conditions.

The thermal relaxation of the system temperature T going from T_1 to T_2 at infinite time can be characterized as

$$T(t) = T_1 + (T_2 - T_1)[1 - \exp(-\gamma t)], \tag{1}$$

in which t is the time and γ is the relaxation rate from the nonequilibrium state. Thus increasing of the relaxation rate can quicken the thermal relaxation. For thermal relaxation between two slabs, the relaxation rate can be defined as

$$\gamma = \frac{\pi^2}{2}\frac{D_T}{w^2}, \tag{2}$$

where D_T is the thermal diffusivity and w is the slab thickness.[20] Thus, a thinner slab will have a larger relaxation rate. In the extreme, an individual molecule in a system can most easily reach equilibration. Therefore, an individual molecule should be heated or cooled rather than an entire

[a)]Author to whom correspondence should be addressed. Tel.: +86-10-62781610. FAX: +86-10-62781610. Electronic mail: caoby@tsinghua.edu.cn.

 © 2008 American Institute of Physics

Downloaded 21 Aug 2008 to 166.111.36.3. Redistribution subject to AIP license or copyright; see http://jcp.aip.org/jcp/copyright.jsp

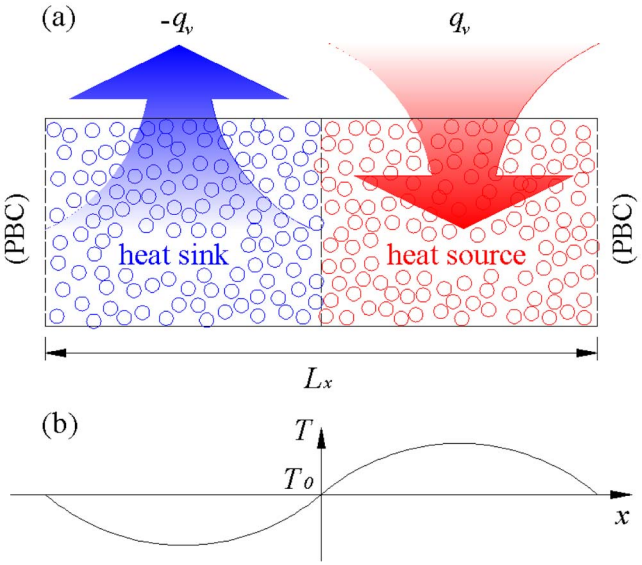

FIG. 1. (Color online) Schematic of (a) the NEMD simulation system applying the relaxation-improved source-and-sink scheme and (b) the temperature profile for periodic boundary conditions.

slab region in a NEMD scheme for calculating the thermal transport.

Thus, a new NEMD scheme based on the heating and cooling of individual molecules is developed to calculate the thermal conductivity to improve relaxation of the thermal perturbation. The thermal perturbation energy either added into or removed from the system is generated based on a Maxwell distribution function generator. The perturbation energy is put into only a few individual molecules each calculation step to improve the thermal perturbation relaxation. The added and removed energy is distributed uniformly throughout the right and left halves of the system. This uniform source and sink scheme leads to a quadratic temperature distribution that is almost sinusoidal. Then, the thermal conductivity can be very easily extracted using Fourier's heat conduction law. The thermal conductivities of liquid and solid argons are calculated to ascertain the convergence, accuracy, and size effect characteristics of the scheme. The theory and methodology are described in Sec. II. This uniform source and sink based NEMD method is then used to calculate the thermal conductivity of molecular liquids and solids taking argon as an example.

II. THEORY AND METHODOLOGY

A schematic for applying the uniform heat source and sink scheme to the NEMD simulations is given in Fig. 1. Periodic boundary conditions (PBC) are used along the x, y, and z directions. The simulation cell is $L_x \times L_y \times L_z$. The thermal energy perturbation forms a uniform heat source throughout the right half of the system and a uniform heat sink throughout the left half, as shown in Fig. 1(a). For a one dimensional problem, the temperature profile is governed by Fourier's heat conduction law,[21]

$$\rho c \frac{\partial T(x,t)}{\partial t} = \lambda \frac{\partial^2 T(x,t)}{\partial x^2} + q_v, \tag{3}$$

where ρ is the mass density, c is the heat capacity at constant pressure, q_v is the energy generation rate (i.e., energy generation per time per volume, with a negative value meaning the energy removal rate), and λ is the thermal conductivity. For steady state, one dimensional conduction, the temperature profile in the x direction can be expressed as

$$T = \begin{cases} \dfrac{q_v}{2\lambda}\left(x + \dfrac{L_x}{4}\right)^2 - \dfrac{q_v {L_x}^2}{32\lambda} + T_0 & \left(-\dfrac{L_x}{2} \leqslant x < 0\right) \\ \dfrac{-q_v}{2\lambda}\left(x - \dfrac{L_x}{4}\right)^2 + \dfrac{q_v {L_x}^2}{32\lambda} + T_0 & \left(0 \leqslant x \leqslant \dfrac{L_x}{2}\right). \end{cases} \tag{4}$$

The uniform heat source and sink with periodic boundary conditions lead to almost sinusoidal with a mean temperature T_0, as shown in Fig. 1(b). Note that this temperature distribution has continuous derivatives across the entire system. The continuity of the temperature and its gradients eliminates the virtual walls that occur in hot and cold slabs usually used in NEMD schemes.

The energy injection and removal are imposed on individual molecules to improve the thermal relaxation. The perturbation energy should be similar to thermal noise. The familiar velocity rescaling and potential cutoff methods can generate noiselike stochastic energy. Unfortunately, the velocity rescaling method cannot generate an ideal uniformly distributed energy perturbation due to the inhomogeneous temperature distribution in NEMD simulations. Thus, we apply a type of stochastic energy perturbation based on the Maxwell distribution,

$$f(\varepsilon_n) = \left(\frac{8m}{\pi}\right)^{1/2} \frac{\varepsilon_n}{(k_B T_n)^{3/2}} \exp\left(-\frac{\varepsilon_n}{T_n}\right). \tag{5}$$

Here ε_n is the thermal perturbation energy, m is the mass of an atom, k_B is the Boltzmann constant, and T_n is a reference temperature for generating the thermal perturbation, where $T_n = 0.01 T_0$ is used here so that the thermal perturbation signals are very small compared to the system mean temperature. The thermal perturbation energy is imposed on several individual molecules at each calculation step with the molecules randomly chosen to keep the heat source and sink distributed uniformly. When an amount of thermal perturbation energy is added onto a molecule in the heat source region, i.e., the right half of the system, an equal amount of energy is removed from another molecule in the heat sink region at the same time. Thus, the equal energy generation and removal densities are equal. The heat source and sink densities can be given as

$$q_v = \frac{2\Sigma_l \varepsilon_{nl}}{\Delta t L_x L_y L_z}, \tag{6}$$

in which $\Sigma_i \varepsilon_{ni}$ is the total thermal perturbation energy added or removed in half of the system during the simulation time Δt.

Downloaded 21 Aug 2008 to 166.111.36.3. Redistribution subject to AIP license or copyright; see http://jcp.aip.org/jcp/copyright.jsp

TABLE I. Rescaled units for the physical parameters used in the MD simulations. k_B is the Boltzmann constant. The physical parameters using rescaled units are indicated by a superscript " *."

Parameter	Temperature (T^*)	Numerical density (n^*)	Time (t^*)	Velocity (v^*)	Thermal conductivity (λ^*)	Energy source density (q_v^*)
Rescaled unit	ε/k_B	σ^{-3}	$\tau=\sigma(m/\varepsilon)^{1/2}$	σ/τ	$k_B/(\sigma\tau)$	$\varepsilon/(\sigma^3\tau)$

From Eq. (4), the mean temperatures of the left and right halves of the system are

$$\bar{T}_L = T_0 - \frac{2}{L_x}\int_{-L_x/2}^{0} T(x)dx = T_0 - \frac{q_v {L_x}^2}{48\lambda}, \tag{7a}$$

$$\bar{T}_R = T_0 + \frac{2}{L_x}\int_{0}^{L_x/2} T(x)dx = T_0 + \frac{q_v {L_x}^2}{48\lambda}. \tag{7b}$$

The average temperature difference between the left and right mean system temperatures, i.e., $\bar{T}_L$ and $\bar{T}_R$, and the system mean temperature T_0 is then

$$\overline{\Delta T} = \frac{(T_0 - T_L) + (\bar{T}_R - T_0)}{2} = \frac{q_v {L_x}^2}{48\lambda}. \tag{8}$$

Thus, the thermal conductivity can then be extracted from the left and right mean system temperatures, i.e., $\lambda = q_v {L_x}^2/48\overline{\Delta T}$. This calculated thermal conductivity is an average over a range of temperatures and densities due to the inhomogeneities in the temperatures and densities in NEMD systems, which is a weakness of most NEMD methods when calculating the thermal conductivity.[8–14] Note that this method for calculating the thermal conductivity does not need the local temperatures of all the slabs with a curve fit of the temperature profile as in other NEMD schemes. Calculation of the left and right mean system temperatures in this NEMD scheme will then much more easily converge with smaller uncertainties than in other NEMD methods.

III. SIMULATION RESULTS AND DISCUSSION

The uniform heat source and sink scheme has been used to calculate the thermal conductivity of liquid and solid argons. Argon is simulated because its atomic dynamics can be described with very good accuracy by a simple Lennard-Jones (LJ) pair potential with many benchmark results for the thermal conductivity available in previous works. The particle interactions are described by the LJ potential in the form

$$\phi(r) = 4\varepsilon\left[\left(\frac{\sigma}{r}\right)^{12} - \left(\frac{\sigma}{r}\right)^{6}\right], \tag{9}$$

where r is the intermolecular distance, ε is the energy parameter, and σ is the molecular diameter. The parameters used in this paper are $\varepsilon=1.67\times10^{-21}$ J and $\sigma=3.41\times10^{-10}$ m.[22] For convenience, rescaled units are used for most physical parameters as indicated by the superscript " *" in Table I.

The molecules move according to Newton's second law. The equations of motion for the molecules are integrated using a leapfrog Verlet algorithm[23] with a timestep of $dt=0.005\tau$. The time-consuming calculations of the interparticle interactions are reduced by using a potential cutoff of $r_{\text{cut}}=2.5\sigma$ and the cell-linked list method. The simulated systems are maintained at a constant temperature by the Nose–Hoover thermostat method.[24–26] The Nose–Hoover equations of motion are

$$\dot{\mathbf{r}} = \mathbf{p}/m,$$

$$\dot{\mathbf{p}} = \mathbf{F} - \xi\mathbf{p}, \tag{10}$$

$$\dot{\xi} = \frac{1}{Q}\left[\sum \frac{p^2}{m} - gk_BT\right].$$

Here $g=3N$ and $Q=3Nk_BT\tau_r^2$ in which τ_r is a relaxation time constant governing the rate at which the equations of motion damp out fluctuations in the kinetic energy. The systems are divided into 25 slabs to calculate the local temperatures. The local temperatures are calculated to show the temperature distribution across the system for examining the uniform heat source and sink based scheme, but they are not necessary for the thermal conductivity calculation.

A. Liquid argon

The liquid argon system contains 1000 molecules. The simulation cell has $L_x:L_y:L_z=2:1:1$ with the actual values determined by the given density for each simulated case. The system mean temperature, density, and heat source and sink density are varied to show the effects of these parameters on the scheme. The heat source and sink density depend on the number of molecules F to which the thermal perturbation energies are added or removed each time step. Thus, F represents the thermal perturbation strength. The temperature distribution is governed by the thermal perturbation strength and the system mean temperature. Each case is run for 1000τ (200 000 time steps) for the system heat conduction to reach steady state. Then the left and right mean temperatures, the local slab temperatures, and the heat source and sink densities are averaged over 1500τ (300 000 time steps). These time lengths are found to be sufficient to obtain converged results as shown below.

Typical temperature and density profiles are shown in Figs. 2(a) and 2(b) for various thermal perturbation strengths characterized by F. The uniform heat source and sink scheme along with the periodic boundary conditions lead to a quadratic temperature profile, as shown in Fig. 2(a). The temperature profiles in both the left and right halves are quadratic and can be fitted by quadratic functions, which agrees with Eq. (4). The deviation of the left and right mean temperatures from the system mean temperature T_0 depends on

Downloaded 21 Aug 2008 to 166.111.36.3. Redistribution subject to AIP license or copyright; see http://jcp.aip.org/jcp/copyright.jsp

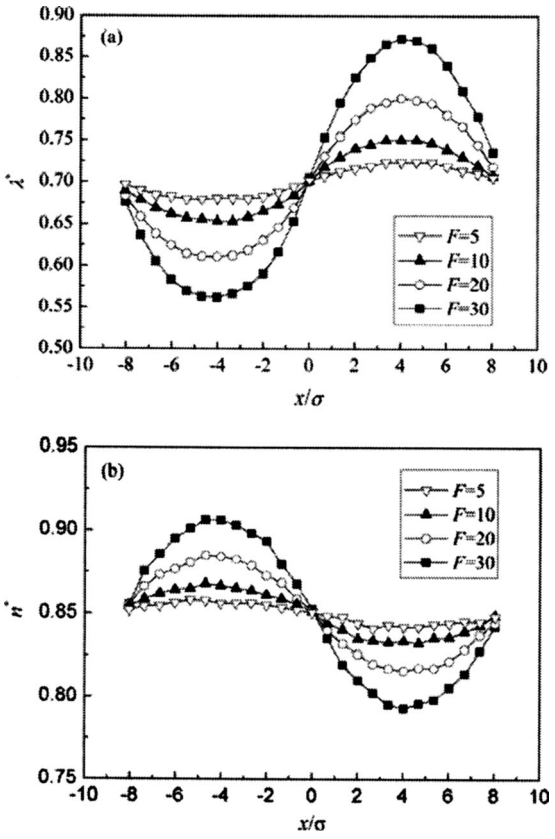

FIG. 2. (a) Temperature profiles and (b) density profiles for various thermal perturbation strengths. The mean system temperature is $T_0^*=0.7$ and the mean density is $n^*=0.85$.

the thermal perturbation strength F. A stronger thermal perturbation always results in larger temperature differences throughout the system. For $F=30$, the temperatures range from 0.55 to 0.90 with a temperature difference of about 0.35. For $F=5$, the maximum temperature difference is less than 0.04 (4.8 K), which is a very small perturbation compared to the system mean temperature, $T_0=0.7$. The left and right mean temperatures can be used to calculate the thermal conductivity of the fluid according to Eq. (7). The statistical error of the left and right mean temperatures can then be used to calculate the errors in the thermal conductivity. The nonuniform temperature profile always leads to a density profile as shown in Fig. 2(b) with smaller temperature differences leading to more homogeneous density distributions.

The time averaged thermal conductivity, heat source density, and left and right mean temperatures are shown in Fig. 3 for $F=10$. The heat source density, as well as the heat sink density (not shown here), has only very slight variations in the simulation average as shown in Fig. 3(b), which indicates that the Maxwell function generates a very stable thermal perturbation energy. The left and right mean temperatures shown in Fig. 3(c) initially have very small fluctuation but then quickly converge. The thermal conductivity average in Fig. 3(a) initially has larger variations than the heat source and sink densities and the left and right mean temperatures due to the uncertainty in calculated transport coefficients arising from statistical errors in both the heat source and sink densities and the left and right mean temperatures, which

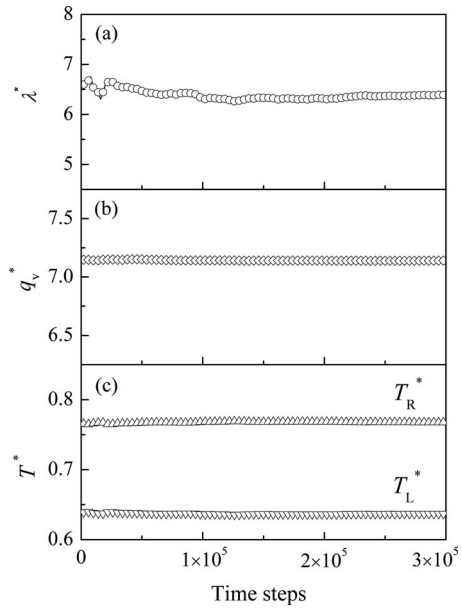

FIG. 3. Time averages for liquid argon simulation for (a) the thermal conductivity, (b) the heat source density, and (c) the left and right mean temperatures.

agrees with the prediction of Eq. (8). The results in Fig. 3 show that the simulations need about 750τ (1.5×10^5 time steps) to obtain a converged result for the thermal conductivity, which is much less than the primary estimate of 5000τ for the reversed NEMD scheme in Ref. 16. These results imply that the left and right mean temperatures converge much faster than data collected in slabs containing fewer molecules.

The dependence of the calculated thermal conductivity on the thermal perturbation strength is shown in Fig. 4. The thermal conductivity uncertainty decreases as the thermal perturbation strength increases with the same averaging time. With $F=2$, the relative uncertainty of the calculated thermal conductivity is about $\pm29\%$. The uncertainty decreases to $\pm4.8\%$ when $F=25$. The first six data points in Fig. 4 for $F\leqq25$ range from 6.3 to 6.8. The last two points are then less than 5.8 and differ greatly from the first six points. Large thermal perturbations, such as $F\geqq25$, can lead to large temperature differences, i.e., inhomogeneities, in these simulations. When the thermal conductivity is averaged over the

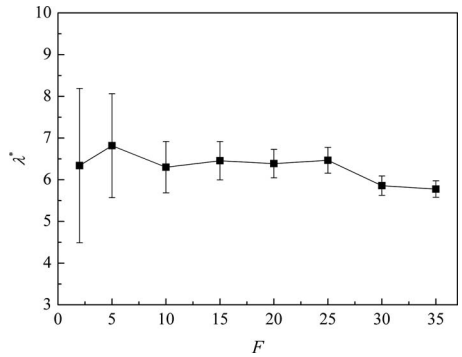

FIG. 4. Dependence of the calculated thermal conductivity of liquid argon on the strength of the applied thermal perturbation, $T_0^*=0.7$, $n^*=0.85$, and an averaging time of 1500τ.

Downloaded 21 Aug 2008 to 166.111.36.3. Redistribution subject to AIP license or copyright; see http://jcp.aip.org/jcp/copyright.jsp

TABLE II. Calculated thermal conductivities and previous data for liquid argon at specified temperatures and numerical densities.

		Thermal conductivity λ*				
T_0^*	n^*	Present work	EMD[a]	EMD[b]	NEMD[c]	Molecular theory[d]
0.9	0.85	6.67 ± 0.38 ($F=15$)	7.28 ± 2.70	7.2	7.2	8.88
1.0	0.75	4.88 ± 0.30 ($F=15$)	5.29 ± 1.85	4.7	5.4	5.55
1.3	0.85	7.14 ± 0.58 ($F=15$)	7.77 ± 2.72	8.0 ($T_0^*=1.32$)	7.9 ($T_0^*=1.32$)	8.73
1.5	0.65	3.87 ± 0.58 ($F=5$)	4.13 ± 1.58	4.1 ($T_0^*=1.59$)	4.1 ($T_0^*=1.59$)	4.36
1.8	0.65	4.05 ± 0.89 ($F=5$)	4.14 ± 1.64	4.5 ($T_0^*=1.85$)	4.3 ($T_0^*=1.85$)	3.96
2.0	0.75	5.46 ± 0.96 ($F=5$)	5.92 ± 2.27	6.1	6.1	6.27

[a]Reference 27.
[b]Reference 28.
[c]Reference 16.
[d]Reference 29.

entire system, these inhomogeneities may result in significant deviations of the results such as shown in Fig. 4 for $F \leqq 25$ from the intrinsic thermal conductivity of the fluid. Therefore, considering the calculational uncertainties and the homogeneity, F should be between 5 and 25 for these simulations.

Table II presents the calculated thermal conductivities of liquid argon for six liquid temperatures and various numerical densities. The results obtained using this uniform heat source and sink NEMD scheme are within 10% of previous results using other MD methods at the same state points. The present results also agree well with the molecular theory results.[29] The thermal conductivity near the triple point is also calculated with $n^*=0.8442$ and $T_0{}^*=0.722$. The present scheme gives the rescaled thermal conductivity as 6.84 ± 0.29, which compares well with the values of 6.5–7.1 obtained using various MD methods.[6,30–33] Thus, the present method is quite accurate and much faster than previous NEMD methods.

B. Solid argon

The solid argon simulations assume that argon is a face-centered cubic crystal with a lattice constant $a=1.5591\sigma$, which corresponds to a numerical density $n^*=1.0554$ of solid argon at a pressure of 5 atm.[34] The lengths of the simulation box in the y and z directions are set to $L_y=L_y=7.8\sigma$, with L_x adjusted to observe the system size effects. The simulations include of 1000–12 000 molecules with L_x ranging from 15σ to 190σ. The other calculation details are the same as those for the liquid argon simulations. The system length, mean temperature, and thermal perturbation strength are varied to examine how effectively the improved relaxation scheme calculates the thermal conductivities of solids. Each run allows 500τ (100 000 time steps) for the system to reach steady state heat conduction, then the left and right mean temperatures, the local temperatures in the slabs, and the heat source and sink densities are averaged over another 500τ (100 000 time steps).

The temperature and density profiles for solid argon are shown in Figs. 5(a) and 5(b) for various system lengths. Smaller thermal perturbations are required for longer systems to maintain a small temperature difference in the system, as can also be demonstrated by Eq. (8). The uniform heat source and sink scheme lead to a quadratic temperature profile that is almost sinusoidal as shown in Fig. 5(a). This indicates that the heat source and sink induced by the thermal perturbations are uniform. As the simulations for liquid argon, larger thermal perturbation strengths increase the temperature difference in the system. For simplicity, the effects of variations of F are not shown here. The thermal perturbation strengths for the various system lengths are selected to ensure that the temperature differences across the simulation system are less than 0.2. In Fig. 5(b), the density profiles are nearly straight horizontal lines. Unlike liquid argon, the density of solid argon is not sensitive to the variation of the

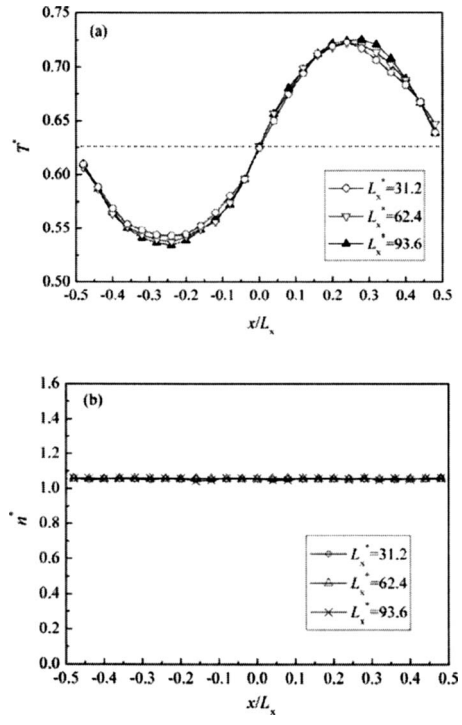

FIG. 5. (a) Temperature profiles and (b) density profiles for various system lengths. The mean system temperature is $T_0{}^*=0.626$ and the mean density is $n^*=1.0554$. For $L_x{}^*=31.2$, $F=25$; for $L_x{}^*=62.4$, $F=20$; and for $L_x{}^*=93.6$, $F=10$.

Downloaded 21 Aug 2008 to 166.111.36.3. Redistribution subject to AIP license or copyright; see http://jcp.aip.org/jcp/copyright.jsp

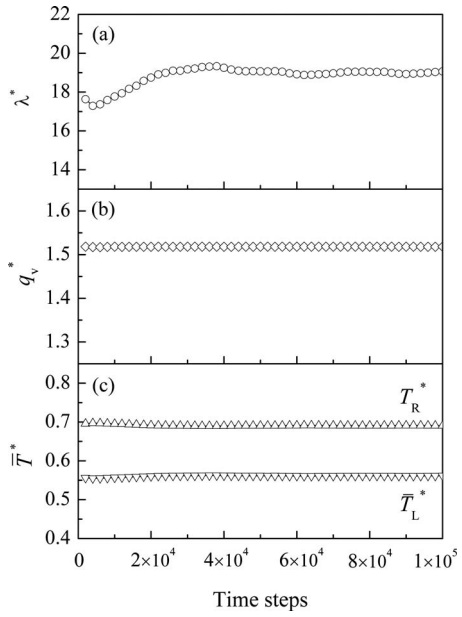

FIG. 6. Time averages for (a) the thermal conductivity, (b) the heat source density, and (c) the left and right mean temperatures for solid argon with $L_x^*=31.2$ and $F=25$.

temperature and remains quite uniform due to the small thermal perturbations and the rather small compressibility of solid argon.

The time average of the thermal conductivity, heat source density, and left and right mean temperatures are shown in Fig. 6 for $L_x^*=31.2$ and $F=25$. As with the liquid argon, the heat source density and the left and right mean temperatures initially have small fluctuations and then converge quickly, as shown in Figs. 6(b) and 6(c). The thermal conductivity again has larger variations in convergence as shown in Fig. 6(a) than the heat source density or the left and right mean temperature averages. The results in Fig. 6 show that only 300τ (6×10^4 time steps) is needed to obtain a stable result, which reflects the rapid convergence of this improved relaxation scheme.

The calculated solid argon thermal conductivities for various system sizes are presented in Fig. 7. Here, the system size is defined as the half width of the system in the x direction (i.e., $L_x/2$). As the system size increases, the thermal

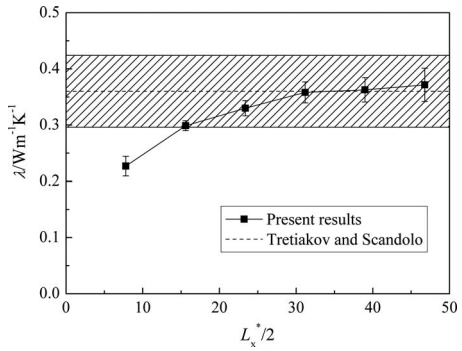

FIG. 7. Dependence of the thermal conductivity of solid argon on the system size. $T_0^*=0.626$, $n^*=1.0554$, and an averaging time of 500τ. The cross-hatched block represents the uncertainty of the EMD results of Tretiakov and Scandolo (Ref. 36).

conductivity increases up to 0.36 W/mK for systems larger than 30σ. The reference value was obtained using an EMD mehod and was demonstrated to have very small size effects.[35] Figure 7 shows that this improved relaxation scheme exhibits size effects for system lengths less than 30σ which can be ignored for larger systems. The size effects arise when the length of the simulation system is not much longer than the phonon mean free path. Strictly speaking, the effects are unavoidable with all MD methods because such methods cannot deal infinitely large molecular systems. Nevertheless, the size effects in the EMD methods are much less than in NEMD methods.[17,35,36] In the standard NEMD methods, the size effects are a result of phonon scattering at the interfaces of the heat source and sink,[37] which indicates that the thermal perturbation changes the state of the phonons. Therefore, the improved thermal relaxation of the thermal perturbation, such as in the present method, can reduce the system size effects. Heino[19] found that the solid argon thermal conductivity calculated using a NEMD method did not converge until the system size reached $11\,450\sigma$ (3900 nm), which would significantly increase the computational cost. The present results show that improving the relaxation of the thermal perturbation as in the present NEMD scheme can significantly reduce the size effects for the thermal conductivity calculations.

The system size dependence of NEMD approaches is often understood to be a result of phonon scattering induced by the heating and cooling slabs. This size effects on the thermal conductivity have been characterized as[17,19]

$$\frac{1}{\lambda}=\frac{2}{nk_Bv}\left(\frac{1}{l_\infty}+\frac{4}{L}\right), \tag{11}$$

where v is the average group velocity of phonons, l_∞ is the phonon mean free path in an infinite system, and L is the system length. The phonon mean free path in an infinite system can be estimated using kinetic theory as

$$l_\infty=\frac{3\lambda}{cv}. \tag{12}$$

Using $c=3nk_B$ and

$$v=\frac{k_B\theta_D}{\hbar k_D}, \tag{13}$$

where n is the number density, $\hbar$ is the Planck constant, $\theta_D=92$ K[38] is the Debye temperature of solid argon, and $k_D=\sqrt[3]{6n\pi^2}/v$ is the Debye wave vector. Then $v=1000$ m/s, which agrees with previous experimental value.[39] For argon at 75 K, l_∞ is about 3σ (1 nm). Thus, the size effects can become very small for system sizes not much longer than the phonon mean free path. This indicates that the physical mechanisms controlling the size effects for the present improved relaxation scheme differ from that of other NEMD methods and that the degree of the size effects depends on the heat resource and sink distributions. In addition, the mean free path of phonons in low-dimensional materials can be quite long, e.g., in the order of micrometers for carbon nanotubes.[40–43] Thus, the improved relaxation NEMD method should be useful for thermal conductivity calcula-

Downloaded 21 Aug 2008 to 166.111.36.3. Redistribution subject to AIP license or copyright; see http://jcp.aip.org/jcp/copyright.jsp

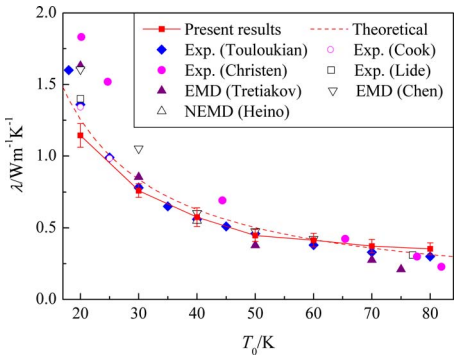

FIG. 8. (Color online) Comparison of calculated thermal conductivity of solid argon at various temperatures with experimental data from Refs. 44 (♦), 45 (○), 46 (●), and 47 (□), and EMD results from Refs. 35 (▲), 36 (▽), NEMD results from Ref. 19 (△) calculated by extrapolating the system size to infinity and a theoretical prediction of $\lambda \sim T^{-1}$ [(---) Ref. 39] combined with previous experimental data (Ref. 44) to determine the coefficient.

tions in such materials due to its small size effects.

The dependence of the calculated thermal conductivity of solid argon on temperature is shown in Fig. 8 for temperatures from 20 to 80 K. The simulation for $T_0=20$ K uses $L_x/2=93.6\sigma$, while other simulations all use $L_x/2=46.8\sigma$. The present results agree well with previous experimental data,[44,45,47] EMD results,[35,36] NEMD results,[19] and theoretical predictions.[39] Note that Heino[19] calculated the thermal conductivity by extrapolating the NEMD system size to infinity. For this temperature range, the deviation of the present results from these previous results is within 15% except for Christen's experimental data[46] at low temperatures less than 50 K. Comparison with the other data in Fig. 8 suggests that his measurements may have some uncertainty. Figure 8 demonstrates that the improved relaxation NEMD scheme can accurately predict the thermal conductivity of solids.

IV. CONCLUSIONS

A NEMD scheme using stochastic energy injection and removal as uniform heat source and sink is developed to calculate the thermal conductivity. The thermal relaxation of the thermal perturbation is better than in other NEMD algorithms because the thermal perturbation energy is only imposed on several individual molecules each time step. The heat source and sink are uniformly distributed in the right and left halves of the system, which leads to a quadratic temperature distribution that is almost sinusoidal. The thermal conductivity can then be easily calculated from the left and right mean temperatures using Fourier's heat conduction law.

The improved relaxation NEMD approach is used to calculate the thermal conductivities of liquid and solid argons. The obtained results agree well with the data and theoretical predictions in the literature. Meanwhile, the very fast improved relaxation scheme is demonstrated to be accurate with small size effects. In addition, other types of energy injection and removal can be used in place of the Maxwell thermal perturbation to make the scheme even more effective.

A few features of the improved relaxation scheme using uniform heat source and sink are worth mentioning. First, there are no heat source and sink slab regions (virtual walls) in the simulation system. In addition, the thermal conductivity can be easily calculated by simply averaging the mean temperatures of each half rather than by fitting temperature profiles. Then, the relaxation of the thermal perturbation is improved because the thermal perturbation energy is only imposed on a few individual molecules. Finally, the improved relaxation NEMD method is expected to be useful for predictions of the thermal conductivity of low-dimensional materials with long phonon mean free paths due to its small size effects.

ACKNOWLEDGMENTS

This work is financially supported by the National Natural Science Foundation of China (No. 50606018).

[1] D. J. Evans and G. P. Morris, *Statistical Mechanics of Nonequilibrium Liquids* (Academic, London, 1990).
[2] M. S. Green, Phys. Rev. **119**, 829 (1960).
[3] H. Mori, Phys. Rev. **112**, 1829 (1958).
[4] R. Kubo, J. Phys. Soc. Jpn. **12**, 570 (1957).
[5] E. Helfand, Phys. Rev. **119**, 1 (1960).
[6] D. J. Evans, Phys. Lett. A **91**, 457 (1982).
[7] M. J. Gillan and M. Dixon, J. Phys. C **16**, 869 (1983).
[8] W. G. Hoover and W. T. Ashurst, Theo. Chem. Adv. Perspectives **1**, 2 (1975).
[9] G. Ciccotti and A. Tenenbaum, J. Stat. Phys. **23**, 767 (1980).
[10] F. Müller-Plathe, J. Chem. Phys. **106**, 6082 (1997).
[11] M. M. Zhang, E. Lussetti, L. E. S. de Souza, and F. Müller-Plathe, J. Phys. Chem. B **109**, 15060 (2006).
[12] R. J. Hulse, R. L. Rowley, and W. V. Wilding, Int. J. Thermophys. **26**, 1 (2005).
[13] T. Terao and F. Müller-Plathe, J. Chem. Phys. **122**, 081103 (2005).
[14] B. Y. Cao, Chin. J. Comput. Phys. **24**, 463 (2007) (in Chinese).
[15] K. Kim and R. Yamamoto, Phys. Rev. E **61**, R41 (2000).
[16] R. D. Mountain, J. Chem. Phys. **124**, 104109 (2006).
[17] P. K. Schelling, S. R. Phillpot, and P. Keblinski, Phys. Rev. B **65**, 144306 (2002).
[18] P. Chantrenne and J. L. Barrat, J. Heat Transfer **126**, 577 (2004).
[19] P. Heino, Phys. Rev. B **71**, 144302 (2005).
[20] B. L. Holian, J. Chem. Phys. **117**, 1173 (2002).
[21] E. R. G. Eckert, *Heat and Mass Transfer* (McGraw-Hill, New York, 1959).
[22] G. C. Maitland, M. Rigby, E. B. Smith, and W. A. Wakeham, *Intermolecular Forces: Their Origin and Determination* (Clarendon, Oxford, 1981).
[23] M. P. Allen and D. J. Tildesley, *Computer Simulation of Liquids* (Oxford University, New York, 1989).
[24] S. Nose, Mol. Phys. **50**, 1055 (1984).
[25] W. G. Hoover, Phys. Rev. A **31**, 1695 (1985).
[26] D. J. Evans and B. L. Holian, J. Chem. Phys. **83**, 4069 (1985).
[27] K. Meier, A. Laesecke, and S. Kabelac, J. Chem. Phys. **121**, 3671 (2004).
[28] R. Vogelsang, C. Hoheisel, and M. Lukas, Mol. Phys. **64**, 1203 (1988).
[29] A. E. Nasrabad, R. Laghaei, and B. C. Eu, J. Chem. Phys. **124**, 084506 (2006).
[30] D. Levesque and L. Verlet, Phys. Rev. A **7**, 1690 (1973).
[31] C. Massobrio and G. Ciccotti, Phys. Rev. A **30**, 3191 (1984).
[32] G. V. Paolini, G. Ciccotti, and C. Massobrio, Phys. Rev. A **34**, 1355 (1986).
[33] S. Viscardy, J. Servantie, and P. Gaspard, J. Chem. Phys. **126**, 184513 (2007).
[34] O. G. Peterson, D. N. Batchelder, and R. O. Simmons, Phys. Rev. **150**, 703 (1966).
[35] K. V. Tretiakov and S. Scandolo, J. Chem. Phys. **120**, 3765 (2004).
[36] Y. F. Chen, J. R. Lukes, D. Y. Li, J. K. Yang, and Y. H. Wu, J. Chem. Phys. **120**, 3841 (2004).

Downloaded 21 Aug 2008 to 166.111.36.3. Redistribution subject to AIP license or copyright; see http://jcp.aip.org/jcp/copyright.jsp

[37] X. G. Liang, Chin. Sci. Bull. **52**, 2457 (2007).
[38] C. Kittel, *Introduction to Solid State Physics*, 5th ed. (Wiley, New York, 1976).
[39] S. Volz, J. B. Saulnier, M. Lallemand, B. Perrin, P. Depondt, and M. Mareschal, Phys. Rev. B **54**, 340 (1996).
[40] P. Kim, L. Shi, A. Majumdar, and P. L. McEuen, Phys. Rev. Lett. **87**, 215502 (2001).
[41] M. Fujii, X. Zhang, H. Q. Xie, H. Ago, K. Takahashi, T. Ikuta, H. Abe, and T. Shimizu, Phys. Rev. Lett. **95**, 065502 (2005).
[42] S. Maruyama, Physica B **323**, 193 (2002).
[43] G. Zhang and B. W. Li, J. Chem. Phys. **123**, 114714 (2005).
[44] *Thermophysical Properties of Matter*, edited by Y. S. Touloukian, P. E. Liley, and S. C. Saxena (IFI/Plenum, New York, 1970), Vol. 3.
[45] *Argon, Helium, and the Rare Gases*, edited by G. A. Cook (Interscience, London, 1961), Vol. I.
[46] D. K. Christen and G. L. Pollack, Phys. Rev. B **12**, 3380 (1975).
[47] *CRC Handbook of Chemistry and Physics*, 79th ed., edited by D. R. Lide (CRC, New York, 1998).

Downloaded 21 Aug 2008 to 166.111.36.3. Redistribution subject to AIP license or copyright; see http://jcp.aip.org/jcp/copyright.jsp